8.A.8 Nuclear Physics B19 (1970) 61-84. North-Holland Publishing Company

A PARTIAL WAVE ANALYSIS OF THE REACTION $K^-n \to \pi^-\Lambda$ IN THE C.M. ENERGY REGION FROM 1900 MeV TO 2100 MeV

G. F. COX, G. S. ISLAM, D. C. COLLEY, D. EASTWOOD, J. R. FRY and F. R. HEATHCOTE
Department of Physics, University of Birmingham

D. J. CANDLIN, J. G. COLVINE, G. COPLEY, N. E. FANCEY and J. MUIR
Department of Natural Philosophy, University of Edinburgh

W. ANGUS, J. R. CAMPBELL, W. T. MORTON and P. J. NEGUS
Department of Natural Philosophy, University of Glasgow

S. S. ALI, I. BUTTERWORTH, F. FUCHS, D. P. GOYAL, D. B. MILLER, D. PEARCE and B. SCHWARZSCHILD
Department of Physics, Imperial College of Science and Technology, London

Received 4 December 1969

Abstract: Results are presented for a partial wave analysis of the reaction $K^-n \to \pi^-\Lambda$ covering a range of c.m. energies from 1900 to 2100 MeV. The events used were obtained from interactions of the type $K^-d \to \pi^-\Lambda p_S$. The analysis was performed both for a sample of events where p_S, the spectator proton from the deuteron, was seen, and for all events. Good agreement was found between the two sets of results. Values of the resonance parameters of the $\Sigma(2030)$ were determined, and some evidence was found supporting the existence of the F5 $\Sigma(1915)$. In addition, the P3 amplitude was found to be rapidly changing near 2100 MeV, consistent with a resonance in this wave at 2080 MeV.

1. INTRODUCTION

Several Σ-resonances have been reported to exist in the energy region 1800-2200 MeV (ref. [1]). Of these, the $\Sigma(2030)$ with spin parity $J^P = \frac{7}{2}^+$ is well established [2-6]. Positive evidence for a $\Sigma(1915)$ with $J^P = \frac{5}{2}^+$ has been found in total cross-section data [2,4] and in an analysis of several formation experiments [5]. Other formation studies [7-10] extending up to a c.m. energy of 1900 MeV have proved insensitive to this effect. However, a recent production experiment [11] suggests a resonance, $\Sigma(1940)$, with parameters different from those of the $\Sigma(1915)$. In particular there is a strong disagreement between the ratios of the $\pi\Lambda$ and $\pi\Sigma$ branching fractions for the

two resonances. From the available evidence it is not clear whether the $\Sigma(1915)$ and $\Sigma(1940)$ are two separate states. A resonance, $\Sigma(1880)$, with $J^P = \frac{1}{2}^+$ has also been suggested [5].

In this paper we present results of an energy-dependent partial wave analysis of the pure $I = 1$ reaction $K^- n \to \pi^- \Lambda$ covering the c.m. energy region from 1900 to 2100 MeV. The data, which are new, consist of the cross-section, angular distribution and Λ-polarization as functions of energy and have been obtained by use of a deuterium filled bubble chamber.

2. EXPERIMENTAL DETAILS

2.1. *The beam*

The experiment employed the Saclay 80 cm bubble chamber filled with liquid deuterium and placed in a separated K^- beam obtained from a target inside NIMROD at the RHEL. Two exposures were made, at beam momenta of 1.45 and 1.65 GeV/c and yielding, respectively, 3.0 and 1.6 events per μb from a total of approximately 700 000 pictures. By virtue of the internal motion of the nucleons in the deuteron, just these two exposures enable us to study $K^- n$ interactions over a range of c.m. energy from 1850 MeV to 2150 MeV. The beam had a momentum resolution of $\pm 1\%$ found by kinematically fitting τ-decays occuring inside the chamber.

2.2. *Scanning, measuring and fitting*

The film was scanned twice for all events except those with only one or two charged tracks at the production vertex and no associated V^0 decay. Events with an odd number of prongs or with a visible slow proton were selected as possible $K^- n$ interactions and were measured on SMPs or conventional film plane digitisers. They were then analysed using either the RHEL or CERN geometrical reconstruction and kinematical fitting programmes.

When the spectator proton from the deuteron was not visible, fits were made by inserting at the production vertex a proton with momentum components $p_x = p_y = p_z = 0$ and standard deviations $\Delta p_x = \Delta p_y = \frac{3}{4}\Delta p_z = 30$ MeV/c. This procedure worked well when the spectator was the only missing particle in the final state, yielding fitted quantities slightly more accurately than a 1c fit made without the constraints.

The fitted, inserted spectators are distributed approximately isotropically in space and have a momentum distribution joining smoothly onto that for seen spectators and agreeing qualitatively with the distribution predicted by the Hulthèn wave function for the deuteron.

3. SELECTION OF $K^- n \to \pi^- \Lambda$ EVENTS

For the present analysis useful events are those having a V^0 decay and either just one prong at the production vertex or two prongs one of which is a slow proton.

3.1. *Treatment of the* Λ/Σ^0 *ambiguity*

A serious problem in selecting a reliable sample of events arose because of the possibility of a given event fitting both the hypothesis being studied in this work, namely

$$K^-d \to \pi^-\Lambda p, \quad (\Lambda \to \pi^- p), \tag{1}$$

and the hypothesis

$$K^-d \to \pi^-\Sigma^0 p, \quad (\Sigma \to \Lambda\gamma,\ \Lambda \to \pi^- p). \tag{2}$$

This ambiguity is especially severe when the spectator proton is not seen: approximately 40% of the seen spectator events and 60% of the unseen spectator events are ambiguous in this way. Partly in view of this, the sample of events with a seen spectator, has been analysed separately from the total sample. We have treated the ambiguity by use of the distribution in $\cos\alpha$, where α is the angle between the decay γ in the Σ^0 rest frame and the Σ^0 line of flight. For genuine decays this should be isotropic but experimentally the distribution for the ambiguous events has a very large peak corresponding to backward going γs. These γs have low laboratory momentum and are presumably due to events really of type (1) but kinematically compatible with reaction (2), within the measurement errors. To remove genuine Σ^0 events while keeping as many true Λs as possible, only events in the backward peak i.e. with $-1.0 < \cos\alpha < -0.8$ are included in our $\pi^-\Lambda p$ sample. The complete sample of events thus obtained (with both seen and unseen spectators) contains an estimated 1.5% contamination of true Σ^0 events and the number of genuine Λ events excluded amounts to roughly 15% of the total.

3.2. *Selection of* K^-n *interactions*

Approximately 20% of the fits to reaction (1) have a proton with laboratory momentum greater than 280 MeV/c, compared with the 1.5% expected from the Hulthèn wave function. These fast spectator events presumably arise from interactions of the incident kaon with the deuteron as a whole or from interactions with a single nucleon where one of the interaction products subsequently reacts with the other nucleon from the deuteron. Accordingly these events are excluded from the analysis. This latter type of reaction sequence is believed to be responsible for the Λp enhancement observed near 2130 MeV (ref. [12]) in experiments at lower beam momenta and also present in this experiment. The enhancement observed by us, is clearly defined for spectator momenta as low as 200 MeV/c and any fit with $2120 < M(\Lambda p) < 2160$ MeV and $p_S > 200$ MeV/c has been discarded.

3.3. *Weighting of* $K^-n \to \pi^-\Lambda$ *events*

Events remaining after application of the cuts described above are taken to represent interactions of an incident kaon with the neutron in the deuteron of the type $K^-n \to \pi^-\Lambda$. To correct for events lost due to Λ-decays outside the selected fiducial region or too close to the production vertex for the event to be correctly identified during scanning, a weight was calculated for each accepted event. This weight is given by

$$W = (\exp(-ml/pt) - \exp(-mL/pt))^{-1},$$

where p is the laboratory momentum of the Λ and m and t its mass and proper life time respectively; L is the distance from the production vertex to the edge of the fiducial region measured along the Λ line of flight and l is the minimum decay length set for each event to correspond to a length projected onto the plane of the chamber windows of 3 mm. This latter cut off was determined from a study of the lifetime plot for seen Λ's.

4. CROSS-SECTIONS FOR THE REACTION $K^-n \to \pi^-\Lambda$

4.1. *Average cross-sections for each exposure*

Cross-sections were calculated separately for the two exposures after correcting the samples of events selected according to the criteria given above, by the following factors:

(i) 1.53 allow for Λ-decays to neutral particles [1],

(ii) 1.11 to compensate for losses in scanning and processing,

(iii) 1.05 ± 0.01 to correct for Glauber shadowing of the neutron by the proton within the deuteron,

(iv) 1.13 ± 0.05 to allow for events excluded by the cut-off on spectator momentum at 280 MeV/c. As noted above only 1.5% of spectators should have momentum greater than this limit whereas experimentally 12% do, averaged over all channels. Presumably these events arise from interactions involving both nucleons from the deuteron, and we have applied a correction factor of $1/(1.0 - 0.12) = 1.13$ in an attempt to allow for $K^-n \to \pi^-\Lambda$ events lost due to subsequent interaction of the π^- or Λ with the spectator proton,

(v) a correction to allow for contamination of the sample by Σ^0 events.

The millibarn equivalent for each exposure was found by using identified τ-decays and applying appropriate factors.

4.2. *Variation of cross-section with c.m. energy*

Assuming the validity of the impulse approximation the c.m. energy E of the K^-n system for each event is equal to the effective mass of all secondaries (here just the π^- and Λ) except the spectator proton. As already stated the selected sample of events has a continuous distribution in E ranging from 1850 MeV to 2150 MeV. To unfold the neutron cross-section $\sigma(E)$ at energy E, from the observed number of events $N(E)\,dE$ in an interval dE about E we have used the relation

$$N(E)\,dE = E\,\sigma(E)\,dE \int \frac{B(p)\,dp}{p} \int |\phi_H(p_S)|^2 F(p_S)\,p_S\,dp_S .$$

The left-hand side is determined experimentally and the right-hand side can be calculated but for the factor $\sigma(E)$. Comparison of the two yields this latter quantity; p is the beam momentum and $B(p)$ is the distribution of beam momenta, assumed to be Gaussian with a full width of 30 MeV/c for both

exposures. $\phi_H(p_s)$ is the Fourier transform of the Hulthèn wave function for the deuteron, given by

$$\phi_H(p_s) \propto [(p_s^2 + \alpha^2)(p_s^2 + \beta^2)]^{-1},$$

with $\alpha = 45.7$ MeV, $\beta = 238$ MeV (ref. [13]) and p_s the laboratory momentum of the spectator proton, $F(p_s)$ is a flux factor * taking account of the relative motion of the target neutron and incident K^- and is given by

$$F(p_s) = \frac{p^{(n)}}{p} \frac{1}{\gamma^{(n)}},$$

where $p^{(n)}$ is the momentum of the incident K^- in the system where the neutron is at rest and $\gamma^{(n)}$ is the Lorentz factor relating the moving neutron to the laboratory system. From the impulse approximation the momentum of the neutron is equal and opposite to that of the spectator and we put $\gamma^{(n)} = \gamma_s$; F can also be written $(kE)/(pE_s)$ where k is the incident momentum in the K^-n c.m.

To obtain $N(E)\,dE$ when using the above relation, events from both exposures were combined and correspondingly the factor $B(p)$ allowed for both exposures and their different millibarn equivalents. The theoretical side of the expression involves two integrations, one over an appropriate range of spectator momentum p_s (see below) and then another over the distribution of beam momentum. Fig. 1 shows the experimental distribution and the predicted curve both for events with $100 < p_s < 280$ MeV/c only.

The use of a lower cut off on momentum in this part of the work avoided any possible biases due to scanning losses for seen spectators or fitting procedures for unseen ones. In addition it enabled the comparison to be made between predicted and experimental distributions that are much flatter than for all events. For the latter sample the distributions are very sharply peaked about the central energies of the two exposures and systematic errors in either could produce large inaccuracies in the computed cross-sections. The theoretical curve was obtained by integrating at a given E over the above range of spectator momenta or the kinematically allowed region if this is more restrictive. In order to make the comparison and deduce $\sigma(E)$ the whole energy range was divided up into bins each containing roughly 120 events and the theoretical curve was integrated over each bin. The bin boundaries, the number of events per bin and the mean energy of the events in each bin are given in table 1, together with numerical values of the cross-section and $A_0 = \sigma/4\pi\lambda^2$. Here λ is the appropriate incident c.m. wave-length divided by 2π.

The results obtained are also shown in fig. 2 together with values of A_0 from refs. [3] and [20].

* See the appendix for a derivation of this effect.

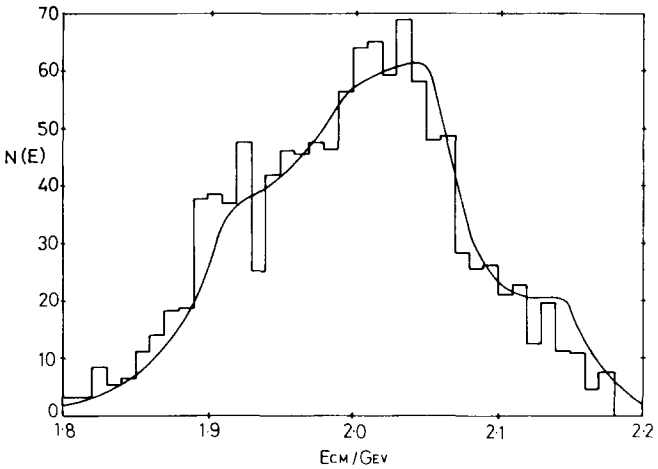

Fig. 1. Experimental and predicted K^-n c.m. energy distributions, for $100 < P_S < 280$ MeV/c. The ordinate shows the number of events per 10 MeV interval and for display the curve has been normalized to contain the same total area as the histogram.

Table 1
Determination of A_0.

Bin limits (MeV)	Mean energy (MeV)	Number of events	σ (mb)	A_0
1850-1900	1881	92	2.88 ± 0.30	0.206 ± 0.021
1900-1930	1915	119	2.46 ± 0.24	0.192 ± 0.019
1930-1960	1947	111	1.88 ± 0.19	0.158 ± 0.016
1960-1990	1976	133	1.94 ± 0.18	0.175 ± 0.016
1990-2010	2000	117	2.19 ± 0.22	0.207 ± 0.021
2010-2030	2020	117	2.15 ± 0.21	0.211 ± 0.021
2030-2050	2040	114	2.13 ± 0.20	0.218 ± 0.021
2050-2080	2063	110	1.78 ± 0.17	0.191 ± 0.019
2080-2160	2113	133	1.74 ± 0.15	0.204 ± 0.018

The errors quoted are purely statistical: each datum has a further normalization error of ±10%.

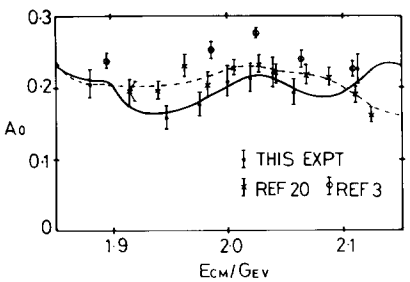

Fig. 2. $A_0 = \sigma/4\pi\lambda\!\!\!^{-2}$, for the reaction $K^-n \to \pi^-\Lambda$. The curves show the predictions of fits 9 (solid line) and 13 (dashed line). The values shown for refs. [3] and [20] were obtained using the relation $\sigma(K^-n \to \pi^-\Lambda) = 2\sigma(K^-p \to \pi^0\Lambda)$.

5. PARTIAL WAVE ANALYSIS

5.1. *Basic formulae*

At a given energy the differential cross-section for the reaction $K^-n \to \pi^-\Lambda$ can be expressed as a series of Legendre polynomials

$$\frac{d\sigma}{d\Omega}(\theta) = \lambda\!\!\!^{-2} \sum_n A_n P_n(\theta),$$

where θ is the c.m. scattering angle defined by $\cos\theta = \boldsymbol{K}\cdot\boldsymbol{\pi}$, where $\boldsymbol{K}$ and $\boldsymbol{\pi}$ are unit vectors along the directions of the K^- and π^- respectively in the K^-n c.m. and the A_n are expansion coefficients.

Likewise the product of the differential cross-section and the polarization of the Λ can be written

$$\frac{d\sigma}{d\Omega}(\theta)\,\boldsymbol{P}(\theta) = \boldsymbol{n}\lambda\!\!\!^{-2} \sum_n B_n P_n^1(\theta),$$

where $\boldsymbol{n}$ is a unit vector parallel to the production normal defined by $\boldsymbol{n} = \boldsymbol{K}\times\boldsymbol{\pi}/|\boldsymbol{K}\times\boldsymbol{\pi}|$, the P_n^1 are first associated Legendre polynomials and the B_n are expansion coefficients.

The coefficients A_n and B_n are bilinear functions of the partial wave scattering amplitudes [15] and form a convenient common meeting ground for experiment and theory.

5.2. *Experimental determination of coefficients*

For each event selected according to the criteria of sect. 3 (without any lower limit on p_S) to be an example of the reaction $K^-n \to \pi^-\Lambda$, the following quantities were calculated: the c.m. energy of the interaction (simply derived from the π^- and Λ variables), the c.m. scattering angle θ, the angle ξ made by the decay proton in the Λ-rest frame with the production normal and the weight of the event as described in subsect. 3.3.

The events were grouped into bins according to c.m. energy, again making use of the deuteron internal motion to study a continuous range of c.m.

energy: the bin sizes, mean positions and numbers of events per bin are given in table 2a. Bins were chosen to contain roughly 200 events so that reasonable determinations of the A and B coefficients could be made, although this made some of the bins rather wide. Also no bin was made less than 10 MeV wide as the energy resolution was not expected to be much better than this amount. Different binning was employed for the two samples of events analysed, namely events with seen spectators and all events. The following procedure applies to both samples. Note that the energy of any bin was taken to be the mean energy of the events in it, not necessarily the central value.

For each bin the quantities A_n/A_0 and B_n/A_0, $n = 1$ to 8 were calculated by the method of moments. Thus

$$A_n/A_0 = (2n+1) \sum w P_n(\theta) / \sum w ,$$

$$B_n/A_0 = \frac{3(2n+1)}{n(n+1)\,\alpha_\Lambda} \sum w P_n^1(\theta) \cos\xi / \sum w ,$$

where the sums extend over all events in a given bin, w is the weight of an individual event and α_Λ was taken to be 0.65 (ref. [1]). Two error matrices were also computed, one for the A_n/A_0 and the other for the B_n/A_0. Fixing

Table 2a
Determination of A_n/A_0, B_n/A_0.

Bin limits (MeV)	Mean energy (MeV)	Number of events	Bin limits (MeV)	Mean energy (MeV)	Number of events
1870-1930	1905	175	1870-1930	1905	176
1930-1965	1950	178	1930-1960	1948	205
1965-1990	1979	180	1960-1975	1968	223
1990-2010	2000	179	1975-1985	1980	265
2010-2030	2020	191	1985-1995	1990	447
2030-2050	2039	208	1995-2005	2000	413
2050-2085	2065	179	2005-2015	2010	357
2085-2150	2113	172	2015-2025	2020	237
			2025-2040	2032	238
			2040-2055	2047	187
			2055-2070	2063	205
			2070-2085	2078	262
			2085-2100	2092	229
			2100-2130	2111	193
Seen spectators only			All spectators		

Table 2b
(A_n/A_0, B_n/A_0, $n = 1, 8$) seen spectators only.

Energy (MeV)	A_1/A_0	A_2/A_0	A_3/A_0	A_4/A_0	A_5/A_0	A_6/A_0	A_7/A_0	A_8/A_0
1905	1.13 ± 0.12	0.57 ± 0.16	-0.65 ± 0.20	-0.67 ± 0.22	0.15 ± 0.25	0.07 ± 0.29	-0.10 ± 0.30	-0.40 ± 0.30
1950	0.88 ± 0.13	0.54 ± 0.16	-0.72 ± 0.20	-0.70 ± 0.23	-0.87 ± 0.24	0.27 ± 0.27	-0.04 ± 0.30	-0.04 ± 0.32
1979	0.48 ± 0.14	0.72 ± 0.17	-0.50 ± 0.21	-0.31 ± 0.25	-1.01 ± 0.26	0.35 ± 0.29	0.03 ± 0.32	0.55 ± 0.34
2000	0.32 ± 0.14	0.64 ± 0.18	-0.04 ± 0.23	0.20 ± 0.25	-0.37 ± 0.27	0.66 ± 0.29	0.38 ± 0.31	-0.33 ± 0.32
2020	0.39 ± 0.14	0.90 ± 0.17	0.17 ± 0.22	-0.07 ± 0.25	-0.76 ± 0.26	0.63 ± 0.28	-0.21 ± 0.31	-0.01 ± 0.33
2039	0.20 ± 0.14	0.70 ± 0.17	0.65 ± 0.21	0.34 ± 0.23	-0.70 ± 0.25	0.49 ± 0.28	-1.07 ± 0.30	-0.12 ± 0.32
2065	0.32 ± 0.14	0.67 ± 0.20	0.88 ± 0.24	1.36 ± 0.26	0.25 ± 0.29	0.74 ± 0.32	-0.08 ± 0.35	0.15 ± 0.37
2113	0.32 ± 0.13	0.09 ± 0.18	0.93 ± 0.21	0.47 ± 0.24	0.22 ± 0.23	0.25 ± 0.26	-0.15 ± 0.29	-0.21 ± 0.30

Energy (MeV)	B_1/A_0	B_2/A_0	B_3/A_0	B_4/A_0	B_5/A_0	B_6/A_0	B_7/A_0	B_8/A_0
1905	0.23 ± 0.24	0.15 ± 0.21	-0.00 ± 0.17	-0.18 ± 0.15	0.06 ± 0.13	-0.02 ± 0.11	-0.08 ± 0.11	-0.07 ± 0.11
1950	-0.14 ± 0.23	-0.44 ± 0.20	-0.47 ± 0.16	-0.42 ± 0.14	-0.20 ± 0.14	-0.20 ± 0.12	-0.17 ± 0.10	0.06 ± 0.10
1979	-0.04 ± 0.21	0.10 ± 0.19	0.14 ± 0.15	0.11 ± 0.13	0.22 ± 0.12	0.05 ± 0.12	0.25 ± 0.11	-0.06 ± 0.10
2000	-0.25 ± 0.23	-0.19 ± 0.19	-0.03 ± 0.16	0.33 ± 0.15	0.18 ± 0.14	0.10 ± 0.13	-0.05 ± 0.12	0.13 ± 0.11
2020	-0.12 ± 0.21	-0.05 ± 0.18	-0.00 ± 0.14	0.33 ± 0.12	0.24 ± 0.12	0.10 ± 0.10	0.09 ± 0.10	-0.00 ± 0.10
2039	0.02 ± 0.21	-0.03 ± 0.17	0.12 ± 0.15	0.45 ± 0.13	0.23 ± 0.12	0.21 ± 0.11	0.11 ± 0.09	-0.01 ± 0.09
2065	-0.03 ± 0.22	0.27 ± 0.16	-0.03 ± 0.16	0.38 ± 0.15	0.06 ± 0.15	0.28 ± 0.13	0.05 ± 0.12	0.12 ± 0.11
2113	0.14 ± 0.26	-0.02 ± 0.19	0.04 ± 0.16	0.28 ± 0.14	0.12 ± 0.15	0.21 ± 0.13	0.06 ± 0.11	-0.08 ± 0.10

Table 2c
(A_n/A_o, B_n/A_o, $n = 1,8$) all events.

Energy (MeV)	A_1/A_o	A_2/A_o	A_3/A_o	A_4/A_o	A_5/A_o	A_6/A_o	A_7/A_o	A_8/A_o
1905	1.13 ± 0.12	0.56 ± 0.16	-0.66 ± 0.20	-0.68 ± 0.22	0.16 ± 0.25	0.10 ± 0.28	-0.09 ± 0.30	-0.42 ± 0.30
1948	0.82 ± 0.12	0.56 ± 0.15	-0.58 ± 0.18	-0.62 ± 0.21	-0.89 ± 0.22	-0.07 ± 0.25	-0.11 ± 0.27	-0.11 ± 0.30
1968	0.13 ± 0.13	0.73 ± 0.15	-0.48 ± 0.18	-0.44 ± 0.22	-0.94 ± 0.22	-0.20 ± 0.26	-0.36 ± 0.28	0.40 ± 0.29
1980	0.26 ± 0.12	0.55 ± 0.14	-0.57 ± 0.18	-0.39 ± 0.20	-0.77 ± 0.22	0.76 ± 0.23	-0.36 ± 0.25	-0.08 ± 0.27
1990	0.36 ± 0.09	0.68 ± 0.11	-0.26 ± 0.14	-0.20 ± 0.15	-0.79 ± 0.16	0.37 ± 0.19	-0.49 ± 0.19	-0.06 ± 0.21
2000	0.08 ± 0.09	0.58 ± 0.11	-0.01 ± 0.14	-0.24 ± 0.16	-0.71 ± 0.17	0.40 ± 0.19	-0.19 ± 0.20	-0.26 ± 0.20
2010	0.55 ± 0.10	0.56 ± 0.12	-0.23 ± 0.15	-0.22 ± 0.17	-0.76 ± 0.18	0.27 ± 0.19	0.03 ± 0.21	-0.04 ± 0.22
2020	0.41 ± 0.13	0.74 ± 0.16	0.15 ± 0.20	0.26 ± 0.21	-0.60 ± 0.24	0.39 ± 0.26	-0.41 ± 0.28	-0.33 ± 0.30
2032	0.39 ± 0.13	0.79 ± 0.16	0.68 ± 0.20	0.30 ± 0.23	-0.46 ± 0.25	0.74 ± 0.27	-0.62 ± 0.29	0.32 ± 0.30
2047	0.22 ± 0.14	0.48 ± 0.18	0.45 ± 0.22	0.45 ± 0.23	-0.91 ± 0.26	0.25 ± 0.30	-1.02 ± 0.30	-0.34 ± 0.34
2063	0.10 ± 0.13	0.20 ± 0.18	0.66 ± 0.22	1.00 ± 0.23	-0.07 ± 0.26	1.08 ± 0.28	0.16 ± 0.30	-0.13 ± 0.32
2078	0.08 ± 0.11	0.09 ± 0.15	0.25 ± 0.19	0.75 ± 0.20	-0.15 ± 0.22	0.74 ± 0.23	-0.32 ± 0.25	-0.36 ± 0.27
2092	0.02 ± 0.11	-0.18 ± 0.15	0.41 ± 0.18	0.45 ± 0.20	-0.29 ± 0.21	0.36 ± 0.23	-0.01 ± 0.25	-0.09 ± 0.26
2111	0.35 ± 0.12	0.06 ± 0.17	1.16 ± 0.19	0.56 ± 0.22	0.26 ± 0.24	0.36 ± 0.25	0.04 ± 0.28	-0.25 ± 0.31
Energy (MeV)	B_1/A_o	B_2/A_o	B_3/A_o	B_4/A_o	B_5/A_o	B_6/A_o	B_7/A_o	B_8/A_o
1905	0.20 ± 0.24	0.12 ± 0.21	-0.00 ± 0.17	-0.16 ± 0.15	0.07 ± 0.13	-0.02 ± 0.11	-0.10 ± 0.11	-0.08 ± 0.11
1948	-0.03 ± 0.22	-0.18 ± 0.18	-0.20 ± 0.15	-0.50 ± 0.13	-0.13 ± 0.12	-0.22 ± 0.11	-0.12 ± 0.10	0.01 ± 0.09
1968	-0.19 ± 0.19	-0.46 ± 0.17	-0.16 ± 0.14	-0.23 ± 0.12	0.20 ± 0.12	-0.06 ± 0.10	0.01 ± 0.09	0.03 ± 0.09
1980	-0.12 ± 0.18	-0.03 ± 0.15	-0.01 ± 0.11	0.09 ± 0.11	0.17 ± 0.10	-0.16 ± 0.09	0.06 ± 0.09	0.01 ± 0.08
1990	-0.32 ± 0.15	-0.02 ± 0.12	0.08 ± 0.10	0.18 ± 0.09	0.30 ± 0.08	0.01 ± 0.08	0.06 ± 0.07	-0.00 ± 0.07
2000	-0.23 ± 0.15	-0.09 ± 0.13	0.26 ± 0.10	0.06 ± 0.10	0.02 ± 0.09	-0.01 ± 0.08	0.05 ± 0.07	0.04 ± 0.07
2010	-0.44 ± 0.16	-0.24 ± 0.13	0.18 ± 0.11	0.17 ± 0.10	0.23 ± 0.09	0.13 ± 0.08	0.08 ± 0.08	-0.02 ± 0.07
2020	-0.35 ± 0.19	0.17 ± 0.16	-0.03 ± 0.13	0.29 ± 0.12	0.13 ± 0.11	0.00 ± 0.10	-0.05 ± 0.09	-0.01 ± 0.09
2032	-0.17 ± 0.19	-0.24 ± 0.16	0.21 ± 0.13	0.43 ± 0.12	0.09 ± 0.11	0.16 ± 0.10	0.01 ± 0.09	-0.16 ± 0.09
2047	0.16 ± 0.22	0.28 ± 0.16	0.19 ± 0.15	0.47 ± 0.14	0.22 ± 0.13	0.29 ± 0.11	0.06 ± 0.10	0.06 ± 0.09
2063	-0.32 ± 0.21	0.11 ± 0.15	0.04 ± 0.13	0.08 ± 0.13	0.07 ± 0.12	0.20 ± 0.11	0.00 ± 0.11	0.07 ± 0.10
2078	-0.24 ± 0.21	0.16 ± 0.14	-0.03 ± 0.12	0.24 ± 0.12	0.28 ± 0.11	0.13 ± 0.11	-0.06 ± 0.10	0.19 ± 0.09
2092	-0.11 ± 0.22	0.11 ± 0.16	0.17 ± 0.13	0.20 ± 0.12	0.10 ± 0.11	0.17 ± 0.10	-0.06 ± 0.09	-0.17 ± 0.09
2111	0.06 ± 0.24	0.28 ± 0.16	0.04 ± 0.14	0.38 ± 0.13	0.37 ± 0.12	0.12 ± 0.12	0.13 ± 0.10	-0.05 ± 0.10

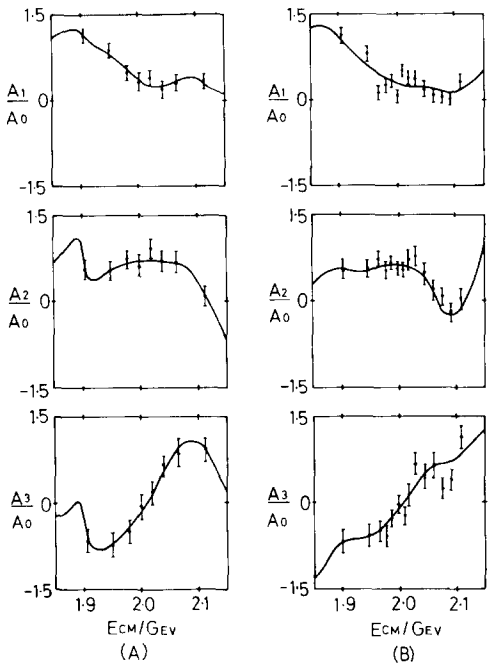

Fig. 3. Experimental and fitted values of A_n/A_0, $n = 1, 3$ for, (A) seen spectator events only with predictions of fit 9, (B) all spectators with predictions of fit 13.

the maximum value of n at 8 is consistent with assuming that only up to G-waves take part in the interaction in our energy region.

Figs. 3-6 show the data from both samples plotted as functions of energy. The curves show the fitted values of fits 9 and 13 described in sect. 6.

Use of the ratios A_n/A_0 and B_n/A_0 confines the normalization errors to the quantities A_0 which were determined as described in sect. 4.

5.3. *Parametrization of the partial wave scattering amplitudes*

An energy dependent partial wave analysis requires as a starting point, parametric forms of the partial wave scattering amplitudes as functions of energy. The amplitude in a given partial wave can be either "resonant" or "non-resonant" (also called "background") or some combination of both.

A purely resonant amplitude T_R can be described as a function of energy by the well known Breit-Wigner formula

$$T_R = e^{i\phi} \frac{(x_e x_r)^{\frac{1}{2}}}{2(E_R - E)/\Gamma - i}.$$

Physically the phase ϕ has to be either 0 or π but in cases in the present work where the choice was uncertain it was allowed to be a variable param-

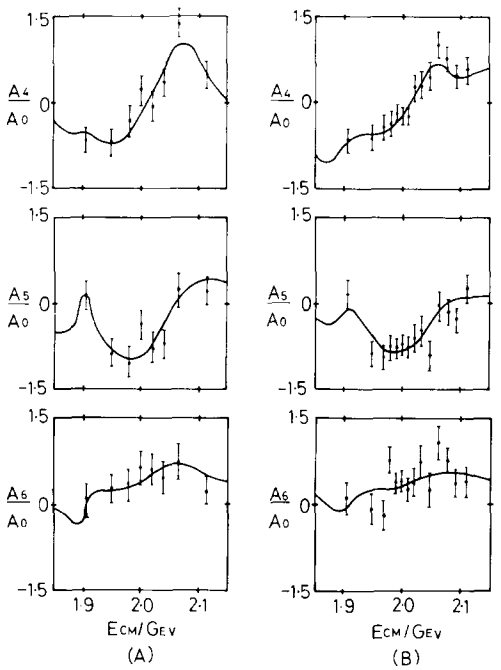

Fig. 4. Experimental and fitted values of A_n/A_0, $n = 4, 6$ for, (A) seen spectator events only with predictions of fit 9, (B) all spectators with predictions of fit 13.

eter [16], E_R is the resonance energy, $x_e = \Gamma_e/\Gamma$ and $x_r = \Gamma_r/\Gamma$ where Γ_e and Γ_r are the partial widths of the resonance in the elastic and reaction (here $\pi\Lambda$) channels respectively and Γ is the total width of the resonance given by

$$\Gamma = \sum_i \Gamma_i ,$$

the sum extending over all open channels. The partial widths have an energy dependence which we assume to be [17] (a test showed this energy dependence to be unimportant)

$$\Gamma_i(E) \propto \left[\frac{k_i^2}{k_i^2 + X^2}\right]^{l_i} \frac{k_i}{E},$$

where k_i and l_i are the c.m. momentum and orbital angular momentum of the decay products of the resonance in the ith channel and X, which is related to the radius of interaction, is taken to be 175 MeV (ref. [5]). In the present work the above prescription gives Γ_e and Γ_r much the same energy variation (the only difference is in the term k_i) so that the total width is as-

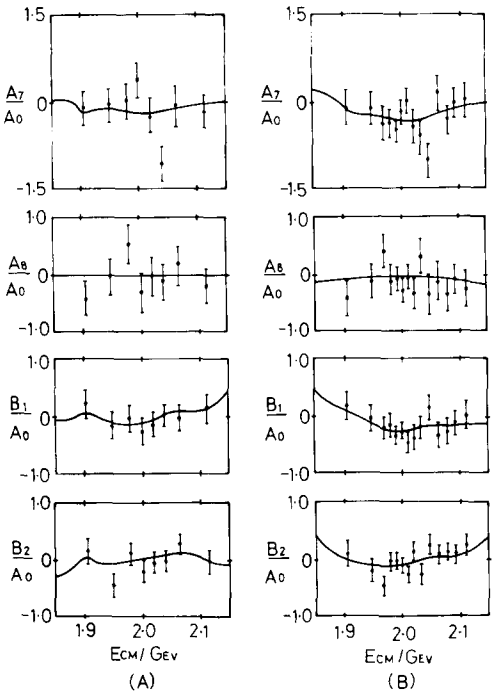

Fig. 5. Experimental and fitted values of A_n/A_0, $n = 7,8$ and B_n/A_0, $n = 1,2$ for, (A) seen spectator events only with predictions of fit 9, (B) all spectators with predictions of fit 13.

sumed to have the energy dependence of Γ_e and the ratios x_e, x_r are assumed to be independent of energy. Thus, possible variable parameters in a resonant amplitude were $(x_e x_r)^{\frac{1}{2}}$, E_R, $\Gamma_R = \Gamma(E_R)$ and ϕ.

There is no widely accepted form governing the energy behaviour of non-resonant or background amplitudes comparable to the Breit-Wigner formula in the resonant case. In the past various groups have tried several different parametrizations (see for example refs. [5, 6, 8]). Here we choose to express the real and imaginary parts of a background amplitude as power series in k, the c.m. momentum in the incident elastic channel. The coefficients in the power series are variable parameters to be determined in the analysis. The highest order such power series used was cubic, although in other cases the power series was limited to be quadratic, linear or even just a constant term. When cubic backgrounds were used the fitting was actually done by writing the real or imaginary part of the amplitude as a series of Legendre polynomials (up to third order) in the variable u, defined by $u = (k - \bar{k})/\Delta k$. Here $\bar{k}$ is the average c.m. momentum of our data and Δk is half the full range of c.m. momenta covered. Note that at the ends of the region $k = \bar{k} \pm \Delta k$ and we have $u = \pm 1$. Obviously such a series is equivalent to a simple power series in k, but it was found that some such use of func-

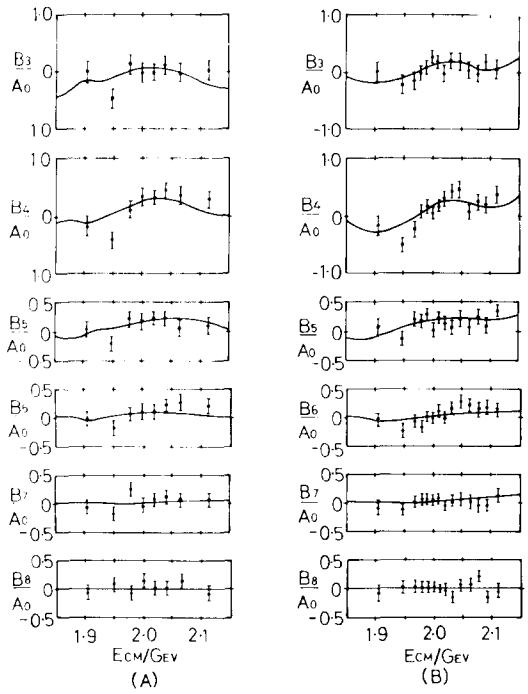

Fig. 6. Experimental and fitted values of B_n/A_0, $n = 3,8$ for, (A) seen spectator events only with predictions of fit 9, (B) all spectators with predictions of fit 13.

tions that are at least approximately orthogonal over the region of data, was essential to reduce the time taken to obtain a fit to reasonable proportions. In general we can write

$$T_B = (A + Bk + Ck^2 + Dk^3) + i(E + Fk + Gk^2 + Hk^3),$$

where the higher-order coefficients are sometimes fixed at zero.

In a partial wave where both resonant and background amplitudes were assumed to exist, the total amplitude was taken to be simply the sum of the two.

5.4. *Fitting procedure*

Given a set of starting values for all parameters used to describe the partial wave amplitudes, the amplitudes themselves and hence the 17 quantities A_0, A_n/A_0 and B_n/A_0, $n = 1$ to 8, can be calculated at each energy for comparison with their experimental values. Fitting was achieved by minimizing with respect to the parameters the overall χ^2 given by

$$\chi^2 = \sum_{ij} (O_i - E_i)(G^{-1})_{ij} (O_j - E_j) .$$

Here O_i and E_i are the observed and expected values of the ith quantity, the sum running over the 17 quantities listed above, at each energy, and G^{-1} is the inverse of the error matrix. All cross correlations between angular and polarization coefficients were taken to be zero. Minimization was carried out using two distinct programmes, one (FMFP) employed the method of Fletcher and Powell [18] and the other (MINROS) the method of Rosenbrock [19].

6. RESULTS

In this section we present and discuss the results of our analysis. The coefficients A_n and B_n obtained using all events show rather greater scatter from energy to energy than do those obtained using only events with a seen spectator. There are no apparent systematic differences between the two sets of coefficients but the increased scatter leads to significantly lower probabilities for fits using all events than for similar fits with seen spectator events only. The two sets of fits otherwise give almost identical results, but we still present the results for the two sets of data separately. Table 3 gives a summary of the most important fits found, the fitted resonance parameters being shown in table 4. All of these fits include a resonant amplitude in the partial wave F7 corresponding to the $\Sigma(2030)$: we were not able to obtain a satisfactory fit without such a resonance. For all of the fits reported, the F7 amplitude was made purely resonant in form with no background, since it was found that, if the sum of a background and resonance is used in this wave, the imaginary part of the background in some fits becomes very much larger than the background in neighbouring waves (e.g. F5 and G7). Such behaviour can be expected with the parametrization employed when the data cover only a portion of the resonant circle. What happens is that the large imaginary background component moves the centre of the resonant circle along the imaginary axis in the Argand diagram and the size of the circle, the position and width of the resonance change to give a total amplitude similar to that for a resonance only. The overall phase ambiguity present in all fits was removed by fixing the phase of this resonance to be π.

6.1. *Fits using only events with a seen spectator*

In fits to seen spectator data only, in addition to the F7 resonance a resonance corresponding to the $\Sigma(1765)$ was imposed in the partial wave D5. However, the parameters of this latter resonance were held fixed at their values in ref. [1] as the data of the present experiment cannot be expected to determine them well. The first group of fits in table 3 uses only constant background amplitudes. Fit 1 with such backgrounds plus fixed D5 and variable F7 resonances is a poor description of the data but was used as a

Table 3
Summary of fits.

Fit	S1	P1	P3	D3	D5	F5	F7	G7	G9	χ^2	NDF	Prob (%)	Data
1	1,1	1,1	1,1	1,1	1,1	1,1	-	1,1	1,1	176.5	118	0.027	
					(R)		R						
2	1,1	1,1	1,1	1,1	1,1	1,1	-	1,1	1,1	146.5	115	2.4	
					(R)	R	R						
3	1,1	1,1	1,1	1,1	1,1	1,1	-	1,1	1,1	146.5	114	2.0	
					(R)	R	R						
4	1,1	1,1	1,1	1,1	1,1	1,1	-	1,1	1,1	153.1	115	0.90	
					(R)	R	R						
5	1,1	1,1	1,1	1,1	1,1	1,1	-	1,1	1,1	136.0	115	8.7	Seen spectators only
	R				(R)		R						
6	1,1	1,1	1,1	1,1	1,1	1,1	-	1,1	1,1	142.6	115	4.0	
			R		(R)		R						
7	1,1	1,1	1,1	1,1	1,1	1,1	-	1,1	1,1	110.5	112	53	
			R		(R)	R	R						
8	2,2	2,2	1,1	1,1	1,1	1,1	-	1,1	1,1	134.9	114	8.7	
					(R)		R						
9	2,2	2,2	1,1	1,1	1,1	1,1	-	1,1	1,1	102.0	108	65	
			R		(R)	R	R						
10	1,1	1,1	1,1	1,1	1,1	1,1	-	1,1	1,1	283.3	208	0.030	
			R		(R)	R	R						
11	4,4	4,4	2,2	3,3	3,3	2,2	-	3,3	3,3	257.5	185	0.025	
			R			R	(R)						
12	4,1	2,4	2,1	2,1	2,3	2,1	-	2,1	2,1	261.2	202	0.27	All events
			R			R	(R)						
13	4,1	2,4	2,1	2,1	2,3	2,1	-	2,1	2,1	257.7	199	0.27	
			R			R	R						
14	4,1	2,4	2,1	2,1	2,3	2,1	-	2,1	2,1	248.5	196	0.59	
			R			R	(R)						

For each fit, the upper line shows the background parametrization used and the lower line shows the resonances included. A background form denoted m,n indicates that the real (imaginary) part contained $m(n)$ variable parameters; e.g. 4,4 implies that both were cubic functions of c.m. momentum. R denotes a variable resonance, (R) a fixed resonance.

starting point to investigate the effects of adding resonances to other waves. Fits 2, 3 and 4 show the results of adding a resonance to the F5 amplitude. With the phase set at zero and a starting mass of 1900 MeV, minimization yielded a fitted mass of 1899 MeV and a reduction in χ^2 of 30.0 for addition of the three variable resonance parameters (fit 2). Starting the phase from $\frac{1}{2}\pi$ and letting it vary along with the other parameters produced (fit 3) the same change in χ^2 with the fitted phase equal to 0.16 ± 0.73 radian and resonance parameters almost identical to those found with the phase fixed at

Table 4
Resonance parameters.

	F7 ($\phi = \pi$)			F5 ($\phi = 0$)			P3 ($\phi = 0$)		
Fit	$\sqrt{x_e x_r}$	E_R	Γ_R	$\sqrt{x_e x_r}$	E_R	Γ_R	$\sqrt{x_e x_r}$	E_R	Γ_R
1	0.16 ± 0.01	2026 ± 6	132 ± 13						
2	0.18 ± 0.01	2027 ± 6	126 ± 15	0.12 ± 0.02	1899 ± 6	55 ± 23			
3 *	0.18 ± 0.01	2027 ± 5	126 ± 14	0.12 ± 0.03	1902 ± 16	61 ± 36			
4	0.18 ± 0.01	2025 ± 5	127 ± 14	‡	‡	‡			
5 †	0.16 ± 0.01	2017 ± 6	131 ± 14						
6	0.16 ± 0.01	2023 ± 7	126 ± 14				0.17 ± 0.04	2117 ± 11	105 ± 41
7	0.19 ± 0.01	2023 ± 6	123 ± 14	0.13 ± 0.02	1898 ± 8	56 ± 23	0.24 ± 0.05	2129 ± 12	94 ± 38
8	0.16 ± 0.02	2023 ± 5	96 ± 13						
9	0.17 ± 0.01	2028 ± 7	128 ± 18	0.10 ± 0.03	1900 ± 5	28 ± 21	0.23 ± 0.06	2129 ± 14	103 ± 50
10	0.19 ± 0.01	2028 ± 5	156 ± 13	0.11 ± 0.02	1895 ± 8	78 ± 25	0.23 ± 0.05	2143 ± 19	144 ± 49
11	0.20	2032	166	0.12 ± 0.05	1894 ± 20	98 ± 42	0.13 ± 0.03	2083 ± 4	81 ± 25
12	0.20	2032	166	0.09 ± 0.02	1904 ± 12	85 ± 28	0.14 ± 0.03	2085 ± 4	81 ± 20
13	0.19 ± 0.01	2027 ± 6	158 ± 16	0.09 ± 0.02	1903 ± 10	77 ± 27	0.16 ± 0.03	2082 ± 4	87 ± 20
14	0.20	2032	166	0.10 ± 0.03	1903 ± 12	83 ± 28	0.14 ± 0.02	2085 ± 4	75 ± 19

* in fit 3 the F5 phase was started from $\frac{1}{2}\pi$ and became 0.16 ± 0.73 rad.
‡ In fit 4 the F5 resonance parameters were 0.08 ± 0.02, 2011 ± 6 and 69 ± 24 with a phase of π.
† In fit 5 the S1 resonance parameters were 0.36 ± 0.12, 2154 ± 31 and 149 ± 62 with a phase of π.

zero. Forcing the phase to be π with a starting mass of 1900 MeV did not produce a solution, the width of the resonance going to zero and the χ^2 only falling to 172.6. A fit was obtained using a phase of π (fit 4) but only when the starting value of the mass was set at 2000 MeV. The fitted F5 total amplitudes in fits 3 and 4 are similar and evidently the two fits represent the same effect in somewhat different ways. The fit with resonance position near 1900 (fit 3) is slightly preferred on the basis of χ^2 and as later fits using all events show a similar but much more marked preference we do not consider fit 4 further.

We next considered the effect of adding a resonance in turn to each of the remaining partial waves. The only cases where the added resonance gives a physical solution with a significant improvement are when the resonance is in the S1 or P3 waves. The S1 resonance (fit 5) gives a reduction in χ^2 of 40.5 but the value of $(x_e x_r)^{\frac{1}{2}}$ found for it is 0.36 ± 0.12. It seems unlikely that if such a strong effect really exists, it has not been observed before. Presumably it can occur here because the "resonance" energy is well beyond the last data. The P3 resonance (fit 6) also produces a large decrease in χ^2, the best fit being found with the phase fixed at zero and mass near 2100 MeV. An alternative fit with phase set at π and a mass of 2000 MeV was not considered acceptable, the χ^2 being 13 higher than for the fit with phase zero. These possible resonances in S1 and P3 both occur near 2100 MeV, however they do not appear to be complementary. When a fit was attempted with resonances added to both S1 and P3, the S1 resonance parameters diverged to totally unacceptable values while the P3 parameters remained similar to those of fit 6. On account of this instability of the S1 resonant amplitude and its overlarge magnitude already mentioned, we do not consider it a candidate for discussion.

The highest probability fit of all using constant backgrounds (fit 7) was obtained with variable resonances in all three partial waves P3, F5 and F7. The χ^2 for this fit is 110.5 for 112 degrees of freedom, considerably lower than for any previous fit and corresponding to a probability of 53%.

The second group of fits in table 3 are those in which linear backgrounds are tried in some waves. Other (e.g. [5]) partial wave analyses have shown that the S1 and P1 amplitudes in particular have considerable energy dependence. Fit 8 shows the result of replacing the constant backgrounds used for these waves in fit 1 by amplitudes with real and imaginary parts linear in c.m. momentum. There is a considerable increase in probability with the χ^2 falling by 41.6: actually most of the effect is produced by the change in parametrization for P1. The fitted amplitude in this wave shows an unexpectedly large dependence on energy over the region covered by our data, though in other respects fit 8 is quite acceptable. Adding the P3 and F5 resonances (fit 9) produces a further fall in χ^2 of 32.9 and leads to a P1 amplitude compatible with those found in other analyses and having a much smaller energy dependence than that found without these resonances. If the resonances are added first as in fit 7, and then the backgrounds made linear, the improvement in χ^2 caused by the change in background form is only 8.5. We are therefore inclined to regard the large P1 variation found in fit 8 as spurious, arising because some energy dependent feature is required to repro-

duce the data in the absence of the effects observed in P3 and F5. The P1 amplitude seems able to do this but only by behaving in an anomalous manner.

If only seen spectator events are used, the quantity of data does not merit the introduction of more complicated background forms, so we terminate our discussion of these events with fit 9.

6.2. *Fits using all events*

A sequence of fits similar to that described above was carried out with the coefficient ratios A_n/A_0, B_n/A_0 obtained using all events. However the threefold increase in statistics that occurs when events with unseen spectators are included, allows more elaborate parametrizations of the partial wave amplitudes to be studied. The most striking feature of these fits is that their probabilities are very much smaller than those obtained with only seen spectator events. For example, fit 10 incorporating resonant amplitudes in the waves P3, D5, F5 and F7 and constant background amplitudes gives a probability of only 0.03%. The corresponding fit to the data from events with seen spectators only (fit 7) has a confidence level of 53%. Actually the total sample of events was divided into 14 energy bins rather than the 8 used for events with seen spectators only. Thus the total number of data is 96 more but the χ^2 in this fit rises by over 170. However the resonance parameters obtained in the two cases are very similar indeed.

As in subsect. 6.1 resonant amplitudes were tried in turn in all partial waves and, further, in some waves several different sets of starting values were employed for the resonance parameters. Again, without listing the many fits carried out, the only possible resonances giving physical solutions with significant improvements in probability and showing stability when the parametrizations of the other waves are altered occur in P3 and F5, with positions of roughly 2100 MeV and 1900 MeV respectively. The alternative F5 resonance at 2000 MeV with a phase of π is only very weak with the present data and is discriminated against by a χ^2 difference of nearly 30.

With the increased number of data it is reasonable to employ more complicated background forms to improve the quality of the fits. In order to constrain these fits to be as physical as possible the following two features were introduced: external A_0 data from published K^-p experiments were sometimes included so that the A_0 data extended roughly 60 MeV beyond the region of our ratio data, at each end (see fits 11, 12 and 13). Secondly, the F7 resonance, being a well established effect, was sometimes held at fixed values derived in an earlier fit (as in fits 11, 12 and 14). Thus fit 11 incorporates variable resonant amplitudes in P3 and F5 and a fixed resonant amplitude in F7 together with the most complicated background parametrizations that can reasonably be expected to occur and at the same time be justified by the quality of the data. As previously stated, the variation of the S1 and P1 background amplitudes was expected to be important, so these were allowed to be cubic functions of c.m. momentum. It was found that when backgrounds of order higher than linear are added to variable resonances, divergences occur so that the background amplitudes in P3 and F5

could only be made linear. Other backgrounds were allowed to be quadratic. Another slightly different feature of fits 11 to 14 is that no fixed D5 resonance corresponding to the $\Sigma(1765)$ was imposed. The reason for this is that although the present data (even using all events) cannot be expected to determine the parameters of this resonance, they may well determine the resonant amplitude in our energy region with a greater precision than can be obtained by using the Breit-Wigner function some way from resonance. Thus the quadratic "background" in D5 describes in fact the total amplitude, resonant plus background. In fit 11 the minimum χ^2 obtained was 257.5 for 185 degrees of freedom, still only a probability of 0.025%. However, many of the higher order background parameters were found to be consistent with zero, and so could be dropped without making the χ^2 of the fit much worse. Thus in fit 12, 17 parameters were removed in this way while the χ^2 increased by only 3.7, giving a probability of 0.27%. The background complexities required by the various partial waves are of some interest: the real part of S1 and the imaginary part of P1 need to be cubic functions of the c.m. momentum, but all the others can be described adequately by linear or even constant forms except in the case of D5 where the $\Sigma(1765)$ is known to act.

The amplitudes found in this fit for the important waves P1 and D5 agree well with those found in other analyses, in particular the D5 amplitude found by us fits nicely onto the resonant circle of the $\Sigma(1765)$. Other waves agree reasonably well except that our P3 amplitude is different from the (background) form found by Smart [5]. Fits 13 and 14 were carried out to check that neither of the two special features introduced above was affecting

Table 5
Background parameters in fits 9 and 13.

		S1	P1	P3	D3	D5	F5	F7	G7	G9
Fit 13	A	0.091	0.160	-0.089	0.095	-0.065	0.049		0.005	0.002
	B	0.021	-0.023	0.052	-0.019	0.029	0.020		0.020	-0.021
	C	-0.034								
	D	0.010								
	E	-0.074	0.034	-0.015	0.028	0.052	-0.009		0.021	-0.017
	F		-0.093			-0.057				
	G		-0.040			-0.026				
	H		0.030							
Fit 9	A	0.103	0.218	-0.071	0.093	0.043	0.038		-0.001	0.010
	B	-0.049	-0.039							
	E	-0.069	0.049	-0.013	0.033	0.051	-0.007		0.016	-0.013
	F	-0.053	-0.031							

The parametrization used was:

$$T_B = (AP_0 + BP_1 + CP_2 + DP_3) + i(EP_0 + FP_1 + GP_2 + HP_3),$$

where P_n is the nth Legendre polynomial in the variable $u = (k - 0.68)/0.0735$ and k is the incident c.m. momentum in GeV/c.
Errors on these fitted parameters are typically 0.02, tending to be somewhat smaller for the higher partial waves and vice versa.

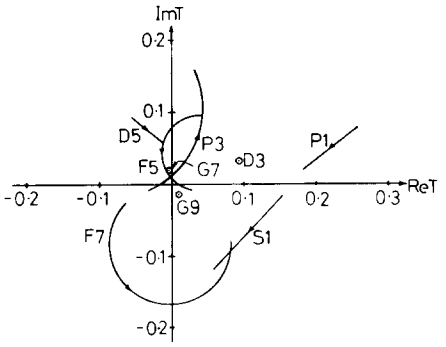

Fig. 7. Argand diagram plot of the fitted partial wave amplitudes from 1900 MeV to 2100 MeV, in fit 9.

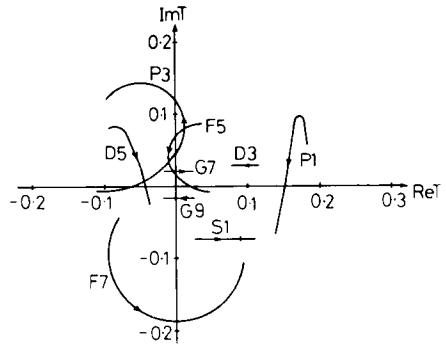

Fig. 8. Argand diagram plot of the fitted partial wave amplitudes from 1900 MeV to 2100 MeV, in fit 13. From its position at 1900 MeV the S1 amplitude initially moves towards the right of the Argand diagram. At about 2000 MeV it reverses its direction and reaches the point marked at 2100 MeV.

the conclusions materially Thus fit 13 is a repeat of fit 12 with the three F7 resonance parameters allowed to vary. The χ^2 fell by 3.5 yielding the same probability of 0.27% and the resonance parameters are hardly changed, in F7 as well as in P3 and F5. Fit 14 used just our own 9 A_0 data rather than the collection of data used in fits 11, 12 and 13. Again, effectively the same fit was obtained showing that any conclusions to be drawn are truly based on our own independent data. The somewhat improved probability of this last fit, namely 0.59% is still not high, but the χ^2 of 248.5 for 233 data and 37 variable parameters shows that the fit represents a reasonable description of our data.

The fitted amplitudes from fits 9 and 13 are displayed in figs. 7 and 8, respectively.

7. CONCLUSIONS

The dominant feature of the analysis is clearly the $\Sigma(2030)$ with $J^P = \frac{7}{2}^+$. The two sets of fitted parameters for this resonance derived in fits 9 and 13 respectively agree well with each other apart from a slight difference in the width. Our preferred values are those of fit 13 which show excellent agreement with those found by Smart [5]. The width of 158 ± 16 MeV differs somewhat from the world-average value of 120 MeV (ref. [1]), although the fit 9 value is closer at 128 ± 18 MeV.

We also find evidence supporting Smart's conclusions with regard to the $\Sigma(1915)$; again, the agreement between us, over its parameters (including spin-parity assignment) is excellent. However we emphasize that our two lowest energy bins, which presumably determine these parameters, are at roughly 1900 and 1950 MeV respectively. Thus our assertions are mainly based on differences between the coefficients in these two bins. Although the agreement with Smart is encouraging (the two analyses being effectively independent) we feel that more data in the region 1850-1950 MeV are needed to establish this resonance with complete certainty.

As the $\Sigma(1915)$ is out of phase with the $\Sigma(2030)$ at resonance there is a difficulty concerning its SU(3) assignment [21,22].

As for the possible resonance in P3 we note that its parameters depend on the location and number of the A_0 data used. With just our own 9 values it is fitted at a higher mass and with a stronger amplitude. When extra A_0 data are inserted in this region the position is moved down to roughly 2080 MeV and the amplitude though less is still significant. With the position at this lower value and the width at about 80 MeV it is clear from table 2 that at least 6 all spectator bins are affected by this resonance, so in this respect we can feel more confident than in the case of the $\Sigma(1915)$. Also ref. [20] contains similar evidence concerning this wave. Both analyses find the proposed $\Sigma(2080)$ to be out of phase with the $\Sigma(2030)$ at resonance which suggests that it would belong to an SU(3) octet with $\alpha < \frac{1}{2}$ or $\alpha > 1$ (ref. [16]).

Regarding other partial wave amplitudes which we have treated as non-resonant we find reasonable agreement with refs. [5] and [20]. S1, P1 and D5 seem to vary appreciably while the others are approximately constant.

All groups are indebted to the operating crews of NIMROD and the Saclay bubble chamber and to Dr. Alan Segar for help with the beam. The bulk of the data processing was carried out at the University of Glasgow SMP/computing unit.

Members of the collaboration are grateful to the measurers and operators at Glasgow and to the scanning and measuring staffs at the other laboratories. The work was supported by grants from the UK Science Research Council.

APPENDIX

The virtual neutron flux factor

Finding the energy variation of $\sigma_n(E)$, the free $K^- n \to \pi^- \Lambda$ cross section

at c.m. energy E involves a flux factor at the $Kn\pi\Lambda$ vertex that is frequently wrongly neglected in practice.

If σ_d is the $K^-d \to \pi^-\Lambda(p)$ cross section and p and p_s are the laboratory beam and spectator momenta, the impulse approximation gives:

$$\sigma_d \propto \frac{1}{p}\int A^2(K^-n \to \pi^-\Lambda)\ |\phi_H(p_s)|^2 \delta^4(P)\prod_j^{\pi} d^4q_j\, \delta(q_j^2 - mj^2). \tag{1}$$

The invariant vertex amplitude A^2 is taken to approximate its mass-shell pole value giving

$$A^2(E) = E^2 \frac{k_i(E)}{k_f(E)} \frac{d\sigma_n(E)}{d\Omega\ \text{c.m.}}. \tag{2}$$

In the vertex flux factor multiplying this differential cross section $q_i(E)$ and $k_f(E)$ are the initial and final c.m. momenta for physical (or mass-shell) $K^-n \to \pi^-\Lambda$ at energy E;

$$k_i(E) = \sqrt{(E^2 - (m_n - m_k)^2)(E^2 - (m_n + m_k)^2)}/2E. \tag{3}$$

Integrating eq. (1) we get for the laboratory spectator distribution:

$$\frac{d^3\sigma_d}{dp_s} \propto \frac{1}{p}|\phi_H(p_s)|^2\, \sigma_n(E)\, \frac{Ek_i}{\sqrt{p_s^2 + m_p^2}}. \tag{4}$$

The kinematic factor Ek_i/pE_s in eq. (4) which is often wrongly ignored is essentially a K^-n vertex flux factor favouring high E and forward spectators. We see that this results in a departure of the laboratory spectator distribution from isotropy and from the simple $|\phi_H(p_s)|^2$ even if $\sigma_n(E)$ is constant.

Noting that

$$\frac{d^3\sigma_d}{dE\, dp_s} = \frac{Ep_s}{p}\frac{d^3\sigma_d}{dp_s}, \tag{5}$$

and integrating over the beam momentum spread we have finally

$$N(E) \propto E^2 k_i\, \sigma_n(E) \int \frac{B(p)\, dp}{p^2} \int \frac{|\phi_H(p_s)|^2 p_s\, dp_s}{E_s}. \tag{6}$$

REFERENCES

[1] Particle Data Group, Rev. Mod. Phys. 41 (1969) 109.
[2] R. L. Cool et al., Phys. Rev. Letters 16 (1966) 1228.
[3] C. G. Wohl, F. T. Solmitz and M. L. Stevenson, Phys. Rev. Letters 17 (1966) 107.
[4] D. V. Bugg et al., Phys. Rev. 168 (1968) 1466.
[5] W. M. Smart, Phys. Rev. 169 (1968) 1330.
[6] C. Daum et al., Nucl. Phys. B6 (1968) 273; Nucl. Phys. B7 (1968) 19.
[7] R. Armenteros et al., Nucl. Phys. B3 (1967) 592.
[8] R. Armenteros et al., Phys. Letters 24B (1967) 198.
[9] R. Armenteros et al., Nucl. Phys. B8 (1968) 183.
[10] B. Conforto et al., Nucl. Phys. B8 (1968) 265.

[11] V. E. Barnes et al., Phys. Rev. Letters 22 (1969) 479.
[12] D. Cline, R. Laumann and J. Mapp, Phys. Rev. Letters 20 (1968) 1452.
[13] M. J. Moravcsik, Nucl. Phys. 7 (1958) 113.
[14] W. P. Trower, Ph. D. Thesis University of Illinois Report COO-1195-54 (1966).
[15] R. D. Tripp, Proc. of the Int. School of Physics, Enrico Fermi, Varenna 1964, p. 70.
[16] A. Kernan and W. M. Smart, Phys. Rev. Letters 17 (1966) 832.
[17] S. L. Glashow and A. H. Rosenfeld, Phys. Rev. Letters 10 (1963) 192.
[18] R. Fletcher and M. J. D. Powell, Computer Journal 6 (1963) 163.
[19] H. H. Rosenbrock, Computer Journal 3 (1960) 175.
[20] A. Berthon et al., submitted to the Lund int. conf. on elementary particles, 1969.
[21] R. D. Tripp, Rapporteur's talk at the 14th int. conf. on high energy physics, Vienna (1968).
[22] R. Levi-Setti, Rapporteur's talk at the Lund int. conf., 1969. University of Chicago preprint EFI 69-78.